

# Comparative Study of Sr<sup>+2</sup> and Zn<sup>+2</sup> Incorporation in the Biomimetic Coating of a Prosthetic Alloy

Wafa I. Abdel-Fattah<sup>\*,1</sup>, El-Sayed M. El-Sayed<sup>2</sup>, Mona S. Talaat<sup>2</sup> and Alaa Adawy<sup>§,1,2</sup>

<sup>1</sup>Biomaterials Department, National Research Centre, 12311 Dokki, Cairo, Egypt

<sup>2</sup>Physics Department, Faculty of Science, Ain-Shams University, 11566 Abbassia, Cairo, Egypt

**Abstract:** The next great wave of innovation and development for implantable medical devices focuses on surface engineering. This would enhance their performance, restore lost functions and ultimately reduce pain. Biomimetic coating is a promising approach, used in that concern. In the present work, an attempt was made to develop the function of the biomimetic coating rather than the classical biocompatibility. Corrected simulated body fluid, leading the conventional fluid concentration by one half, 1.5 × c-SBF, was prepared with adequate supplement of Sr<sup>+2</sup>, or Zn<sup>+2</sup> according to the permissible therapeutic doses, 0.5 mM. The selection of Sr<sup>+2</sup> and Zn<sup>+2</sup> as additives was owing to their anti-osteoporotic and antimicrobial/bacterial activity respectively. The bioinert discs of titanium aluminum vanadium alloy, Ti-6Al-4V, were pretreated according to our previously developed protocol [Alaa Adawy *et al.* 2009, Biomimetic Coating of Precalcified Ti-6Al-4V Alloy, J. Open Medical Devices, 1(2009)19]. Subsequently, they were soaked in the prepared SBFs. Stepwise surface characterization was assessed using Diffuse Reflectance Infra-red Fourier Transform Spectroscopy, DRIFTS. In parallel, the remnants of the soaking solutions were analyzed chemically by atomic absorption and biochemical kits, and physically by AC electrical conductivity measurements at room temperature. Scanning electron microscopy, SEM, was used to assess surface final morphology post the whole treatment duration. Incorporation of Sr<sup>+2</sup> and Zn<sup>+2</sup> resulted in the growth of calcium deficient apatite of high carbonate content. The former increased the activity of biomimetic deposition while the latter induced more uniformity in the resultant coating.

**Keywords:** Biomimetic, Ti-6Al-4V, strontium, zinc, DRIFTS, electrical conductivity.

## 1. INTRODUCTION

Ti-6Al-4V, is one of the most commonly used alloys in implant dentistry. Owing to its low elastic modulus, 50 - 60% that of Co-Cr alloys, it is soft and readily formed. It has high yield points equal to those of carbon steel. In addition, it's high bending strength (twice that of unalloyed titanium) is coupled with great hardness [1, 2]. These properties resulted in high spring back suitable for retentive forces required for clasp of removable partial dentures or for orthodontic uses. The addition of the alloying elements, aluminum and vanadium, to the bioactive titanium leads to higher strength and reduced ductility.

On the other hand, Hydroxyapatite, HA, (Ca<sub>10</sub>(PO<sub>4</sub>)<sub>6</sub>(OH)<sub>2</sub>) is commonly recorded in the hard tissue replacement operations. HA is a bioactive material with a high biocompatibility [3]. It achieves bone mineralization directly on the implant surface and results in better bone growth, penetration; and greater direct contact between the tissue and the implant surface [4]. This is because of its close resemblance to chemical composition (Ca<sup>+2</sup>/iP ratio) of teeth and bones [5]. A modified form of HA, carbonate apatite comprises about 45% by volume and 65% by weight of

human cortical bone. HA has been clinically applied as a dense, sintered material and as a coating for bioinert metallic implant [6]. Other biologically relevant calcium phosphates, (Ca-P), involve amorphous calcium phosphate (ACP), brushite (DCPD), monetite (MCP), octacalcium phosphate (OCP), calcium pyrophosphate,  $\alpha$  and  $\beta$  tricalcium phosphate ( $\alpha$ -TCP), ( $\beta$ -TCP) and tetracalcium phosphate [7]. Nevertheless, biological apatites, whose B-type carbonate substitution, are nanostructured, comprising unique chemical, physical and electrical properties. Extended research on nanophase apatites is required. Results could provide useful insights for designing bioapatites with optimized performance [8].

Biomimetic deposition is simply an electroless, low temperature, chemical deposition [9]. It is a simple, economic route which gives promising results. Besides, it can be used to coat substrates with porous or complex geometry, and it makes it possible to include organic molecules in the film to induce and accelerate the regeneration of living tissues [10]. Simulated body fluid (SBF) is one of the most well known biomimetic solutions. Several solutions, including SBF, have been reported to aid the deposition of a Ca-P on metallic substrates. Their ionic concentration and pH are similar to those of inorganic constituents in human blood plasma. Not only does the precise deposited Ca-P phase depend on the exact chemical and physical conditions of the soaking solution, but also on the activity of the substrate subjected to the treatment. These studies have attracted extensive research owing to the resultant Ca-P phases that resemble biological mineralization.

\*Address correspondence to this author at the Biomaterial Department, National Research Center, 12311 Dokki, Cairo, Egypt; Tel: 00202-33371414; Fax: 00202- 33370931; E-mail: nrcfifi@yahoo.com

§Current Address: Solid State Chemistry department, IMM institute, Faculty of Science, Radboud University Nijmegen, 6525 AJ Nijmegen, Netherlands

From a physical point of view, this biomimetic coating process is based on the heterogeneous nucleation of Ca-P from SBF, which is supersaturated towards hydroxyapatite around the physiological temperature at pH=7.3 ± 0.1. By this technique, bone-like carbonate apatite could be deposited on titanium implants within 7 days [11]. The classical biomimetic Ca-P coating normally requires an immersion period of about 14-28 days with replenishment of SBF. Recently, efforts have been performed to make this process faster and thus improving its practical utility [12]. According to the classical model of heterogeneous nucleation; by increasing the solution concentration, the supersaturation increases which in turn, decreases the energy required for the heterogenous nucleation of calcium phosphate phase on the titanium alloy. However, the degree of supersaturation shouldn't exceed certain limits. Besides, if the calcifying solutions reach their supersaturation point rapidly, they will lead to Ca-P precipitates in the solution and hold Ca-P coating back from growing on the substrate [13].

Here we present our attempt to enhance the properties of Ti-6Al-4V through uploading additional functions to its coating beside the classical biocompatibility. A trial to incorporate trace ions known for their specific properties is investigated. Their substitution in apatite can have several effects on lattice parameters, crystallinity, dissolution kinetics and other physical properties [14].

Strontium (Sr) is a trace element, has the ability to enhance bone volume and prevent bone loss. It has become widely known in the prevention and treatment of osteoporosis as a ranelate compound [15]. Indeed, it has a dual effect associated with improving postmenopausal osteoporosis by reducing bone resorption and increasing bone formation with an eventual effect of decreasing the risk of fractures [16]. *In vitro* studies revealed that strontium ranelate (SR) has an anabolic and antiresorptive activity which leads to an increase in the collagen and non-collagen protein synthesis, an enhancement in pre-osteoblast differentiation, an inhibition in osteoclast function, along with a reduction in osteoclast function [17]. Beside its chemical analogy to Ca, Sr is a bone seeking element and 98% of the total body Sr content can be found in the skeleton. After administration of Sr salt, it passes through the Haversian capillaries walls by diffusion to reach the bone extracellular fluid and finally deposit in the bone, being adsorbed on the bone apatite surface or substitute Ca in bone crystals. Sr<sup>+2</sup>, having ionic radius (1.13Å) higher than that of Ca<sup>+2</sup> (0.99 Å), its incorporation in bone crystals increases the length of Sr-hydroxyl bond more than that of Ca-hydroxyl. This in turn results in a decrease in the lattice energy, which is inversely proportional to the cohesion distance and, therefore, a subsequent decrease in crystallinity. Thus, Sr incorporation in bone mineral may lead to the modifications in lattice parameters, crystal size, and crystallinity of bone mineral [18,19].

In close resemblance, zinc (Zn) is present in small amounts in the enamel of human teeth and bone. It is probably the most important element in medicine because of its role in as many as 200 enzymes. Elevated concentrations in areas of damaged tissues or inflammatory lesions could enhance the ATP-mediated response [20]. It is well

established as an essential trace element, having stimulating effects on bone formation at low concentrations, and has a potent inhibitory effect on osteoclastic bone resorption *in vitro* [21]. Because of its relatively small ionic radius (0.83Å<sup>+</sup>) with respect to Ca<sup>+2</sup>, Zn<sup>+2</sup> existence in the apatite crystal is oriented to grain boundaries, which favors the *in vivo* release to act as an agent for enhancing bone formation. Thus, it lowers the crystallinity and thus promotes precipitation of apatite particles in SBF [22]. Zn<sup>+2</sup> was also reported to have positive effects by decreasing the inflammatory reaction, increasing the chemotaxis and down-regulating the inflammatory reaction [23].

Below, we present our attempt to explore the possible resultant modifications in the deposition mechanism of a biomimetic apatite layer on activated Ti-6Al-4V surfaces by using Sr<sup>+2</sup>, or Zn<sup>+2</sup> as additives to the biomimetic coating solution. This is investigated by studying the grown biomimetic coats on metallic substrates within 10 days using DRIFTS and SEM. In addition, the remaining solutions after samples withdrawal at each soaking step were chemically analyzed and their Ac -electrical conductivity was measured to follow release/deposition of ions on/from the implant surfaces.

## 2. MATERIALS AND METHODS

Ti-6Al-4V discs were purchased from a local producing company (TUT). All samples have the same dimensions: 29.2mm<sup>3</sup> volume, 64.7mm<sup>2</sup> total surface area and 0.22 gm ±0.01gm weight. They were activated according to the author's previous protocol [24]. Briefly, their surfaces were roughened to an average of 35µm, ultrasonically cleaned, alkali and heat treated and subsequently precalcified.

### 2.1. Preparation of SBF

The SBFs were prepared according to Kokoubo *et al.* [25]. In our approach, they exceed the ionic concentration of the ordinary c-SBF by one half, i.e., 1.5 × c-SBF. The same receipt of our previous research [24] was used in the current work. The incorporation of strontium or zinc ions into the biomimetic solutions was maintained by the supplement of 0.5mM of Sr or Zn through addition of adequate amounts of SrCl<sub>2</sub>·6H<sub>2</sub>O (E. merck, Darmstadt, cryst. extra pure, 99%) or ZnCl<sub>2</sub> anhydrous (WINLAB, UK), respectively. They were added after the supplement of CaCl<sub>2</sub> such that a molar ratio of Ca to either Sr or Zn was maintained at 7.5:1. At 37±1°C, the pH of these two modified solutions: 1.5×Sr-c-SBF and 1.5×Zn-c-SBF, was set at 7.3±1. The reagents used in both solutions' preparation are stated together with their molar concentrations according to the ascending order of their addition in Table 1.

The designed solutions were freshly prepared prior to each soaking procedure. The stability of these solutions is not guaranteed after a week at 4°C.

### 2.2. Biomimetic Coating

Each disc sample was hanged vertically in a closed conical polystyrene screwed test tube containing the corresponding solution. This geometry avoids the aggregation of the solution precipitates -if any- on the sample surface. Subsequently, any recorded apatite phase on its surface should be due to direct nucleation. Replenishment

of the soaking solution was done every 2 days with freshly prepared solution. This was repeated up to a total duration of 10 days. After the completion of the soaking periods, the samples were gently rinsed with double distilled water and were left to dry in a desiccator.

**Table 1. Reagents and their Molar Concentrations Used in the Preparation of 1.5 X Sr/Zn-c-SBF**

Order	Reagent	Molar Concentration (mM)
1	NaCl	206
2	NaHCO <sub>3</sub>	6.3
3	KCl	4.5
4	K <sub>2</sub> HPO <sub>4</sub>	1.5
5	MgCl <sub>2</sub> .H <sub>2</sub> O	2.3
6	1M HCl	58.5ml
7	CaCl <sub>2</sub>	4
8	SrCl <sub>2</sub> .6H <sub>2</sub> O or ZnCl <sub>2</sub>	0.5
9	Na <sub>2</sub> SO <sub>4</sub>	0.8
10	(CH <sub>2</sub> OH) <sub>3</sub> CNH <sub>2</sub>	75
11	1M HCl	0-7.5ml

### 2.3. Characterizations

Surface chemical analysis of coated Ti-6Al-4V discs was assessed using DRIFTS (FT-IR 6100 JASCO, DR PRO410-M). Three scans were taken for each sample and the results are the mean values. Spectral resolution is 0.5 cm<sup>-1</sup> and accuracy is within ± 0.01 cm<sup>-1</sup>. Reflectance spectra of the pretreated samples were previously studied [24]. It is supposed that any decrement occur in the solution ions' concentration, is deposition onto sample surface. In reflectance analysis, the optical density for reflectance measurements is given by

$$A_R = -\log T_R \quad (1)$$

Where,  $T_R = I/I_0$  is the reflecting power,  $I_0$  being the intensity of incident radiant energy and  $I$  the intensity of that which reflected by the medium. The DRIFT spectral data can be used to produce spectral plots similar to absorbance spectra by use of the Kubelka-Munk function [26]. In the limit of low concentration of functional groups,  $T_R$ , can be related to the concentration,  $C$ , on the scattering layer through the molar absorptivity,  $\epsilon$ , and the scattering coefficient,  $s$ , as follows:

$$F(T_r) = \frac{(1 - T_r)^2}{2T_r} = \frac{k}{s} = \frac{\epsilon C}{s} \quad (2)$$

Therefore, by applying Kubelka-Munk equation, there is a linear relation between  $T_R$  and the solution concentration for high and moderate concentration but a distinct deviation from linearity is observed for low solution concentration [27]. On this basis, an assessment of the values of the assignment peaks was recorded through the successive soaking periods in order to see the progress in the content of the different functional groups on the alloy surface.

The variation of Ca<sup>+2</sup> and inorganic phosphorus, iP, through successive soaking periods was measured using biochemical kits. For mother solutions, the results of spectrophotometer gave approximately the same concentrations as they were calculated during their preparation and thus confirming the validity of these tests. Spectrophotometer 6100, Type M 129 Jenway LTD - UK was used in absorbance mode. Because the soaking solutions were replenished every two days, at the time of starting each soaking period, equal volume of the same solution was kept under the same conditions without having a sample inside. This "control" sample was used in our final calculations.

Atomic absorption spectroscopy (AVANTA) was used to follow the values of Sr<sup>+2</sup> or Zn<sup>+2</sup> in the soaking solutions. The depletion of these divalent ions from SBF could predict their individual competition vs Ca<sup>+2</sup>.

AC electrical conductivity of soaking solutions was measured after each soaking period with reference to their mother SBF. This procedure is proposed for the assessment of the ionic release or uptake by the treated substrates. A conductance bridge (Griffin and George LTID) and a glass conductance cell made up of fused silica was used. The cell contains two platinum disc electrodes of 0.785 mm<sup>2</sup> in cross section area and separated by a fixed distance at 2mm and connected to the bridge. The samples' codes are given in Table 2.

Morphological investigation of the coated discs was performed using SEM (JEOL JXA-840A electron probe micro analyzer). The samples were sputter-coated with gold before examination. This examination was held with an accelerating voltage of 30KeV.

## 3. RESULTS AND DISCUSSION

### 3.1. DRIFTS

The coating development after successive soaking periods was assessed using DRIFTS. The pretreated sample denoted as SAHPC [24], was used as the initial substrates in this procedure. The samples' codes are given in Table 2.

**Table 2. Sample Notations**

Samples	Time of Soaking in Days			
	4	6	8	10
Sr-c-SBF	Sr-2p*	Sr-3p	Sr-4p	Sr-5p
Zn-c-SBF	Zn-2p	Zn-3p	Zn-4p	Zn-5p

\*p stands for period, each last for 2 days after which the solution was replenished with freshly prepared one.

### 4 Days Soaking

After the vertical immersion of SAHPC in 1.5 × Sr-SBF, or 1.5 × Zn-SBF for two successive soaking periods, i.e., 4 days, an apparent resorption of all the peaks was observed (Figs. 1, 2). All peaks were within the same positions as that of mother sample [24]. In general, the optical density of all the peaks in Sr-c-SBF, (Fig. 1), exceeded those in Zn-c-SBF, (Fig. 2), proving a limited range of resorption in the former with respect to the latter (Tables 3 and 4). A more specific difference was the behavior of the peak value of the "C-O"

stretch  $\nu_3$  mode. It settled around the same value as that of SAHPC in Sr-c-SBF discs. While in Zn-c-SBF, it showed greater decrement.

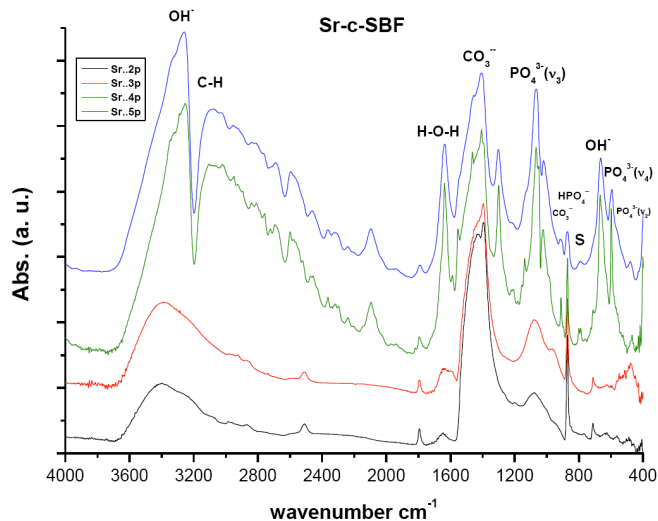


**Fig. (1).** DRIFTS of Sr-c-SBF post 2<sup>nd</sup>, 3<sup>rd</sup>, 4<sup>th</sup> and 5<sup>th</sup> soaking periods in 1.5 X Sr-c-SBF. "S." accounts for the area assigned to Strontianite, SrCO<sub>3</sub>

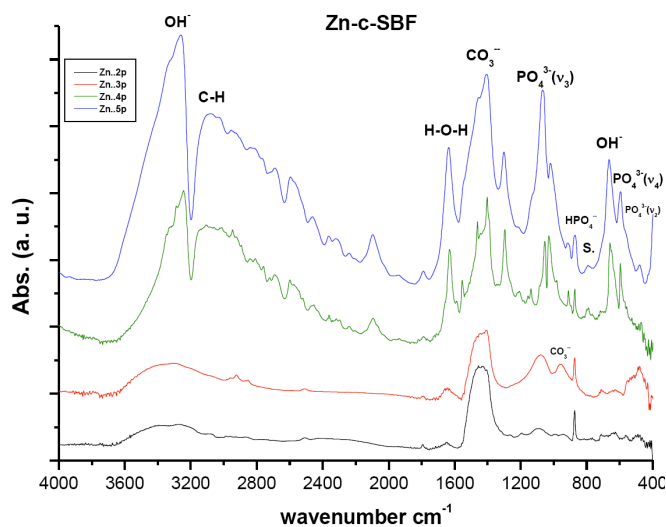


**Fig. (2).** DRIFTS of Zn-c-SBF post 2<sup>nd</sup>, 3<sup>rd</sup>, 4<sup>th</sup> and 5<sup>th</sup> soaking periods in 1.5 X Zn-c-SBF. "S." accounts for the area assigned to Smithsonite, ZnCO<sub>3</sub>

### 6 Days Soaking

A "built in" behavior is shown. This is precisely true for the peaks assigned for OH<sup>-</sup> stretching vibration and PO<sub>4</sub><sup>3-</sup> stretching and bending vibration modes. This growth, whose higher values for Sr-c-SBF than that of Zn-c-SBF, indicates the incorporation of water molecules which accompany the growth of inorganic calcium phosphate phases [14, 28-37]. There was a slight difference detected with respect to the behavior of "out-of-plane" C-O bending vibration  $\nu_2$  band. The band at 871 cm<sup>-1</sup> in Sr-c-SBF, continued its value loss, whereas, at 873 cm<sup>-1</sup> in Zn-c-SBF, it showed a slight increment. Besides, peaks at 712 cm<sup>-1</sup>, (Sr-c-SBF), and at 715 cm<sup>-1</sup>, (Zn-c-SBF) that are assigned to "in-plane" C-O bending vibration, both showed slight decrement. Such peaks as a whole assure the presence of inorganic CO<sub>3</sub><sup>2-</sup>

group [16,21,31-33,36]. In general, the carbonate content at this point showed slight drop on Sr-c-SBF, which was actually as triple in value as that of Zn-c-SBF. In the latter, it stayed around the same values as that measured after 4 days soaking. This indicates a start of the alternative deposition of calcium and phosphate ions in the route of HA formation. The surfaces, at the moment, had already dissolved the extra content of the calcium carbonate phase that was deposited after the fast precalcification step [24]. Being ready for proper calcium phosphate deposition on a calcium rich surface, negatively charged phosphate ions started to show their contribution. Another difference is stated in the presence of the doublet due to the presence of a band around 712 cm<sup>-1</sup> and 623 cm<sup>-1</sup>. This doublet characterizes the growth of aragonite (CaCO<sub>3</sub>) [38]. Strontianite, SrCO<sub>3</sub>, is one of the associated minerals to aragonite. In fact, Sr was reported to substitute Ca in aragonite up to 7500 part/million up to 40% [38]. This in turn explains the stability of carbonate content on Sr-c-SBF which should have been consumed in SrCO<sub>3</sub> growth. In a similar manner, this doublet indicates the growth of smithsonite, ZnCO<sub>3</sub>. It is found as a secondary mineral in the oxidization zone of zinc ore deposits and in sedimentary deposits as a direct oxidization product of sphalerite. Zn can also substitute Ca in aragonite but not as efficiently as Sr [39].

### 8 Days Soaking

The resultant charts showed growth and more differentiation for all the peaks. For both treatments, the water content with the resultant phase had undergone an abrupt increase. In contrast to Zn-c-SBF, it was time of carbonate content inhibition on Sr-c-SBF surface. Nevertheless, the overall value in the former was lower than that in the latter. This was accompanied by growth of phosphate content. The band assigned for PO<sub>4</sub><sup>3-</sup> stretching vibration  $\nu_3$  was as twice in value as that shown post six days soaking. This was true for both treatments. These simultaneous events may be a step in the way of phosphate substitution to the carbonate in the resultant apatite coating. At this moment, it was not clear whether there were sites characteristic for strontianite and smithsonite on Sr-c-SBF and Zn-c-SBF respectively. This is because at these sites two highly differentiated peaks at 667 cm<sup>-1</sup>, on Sr-c-SBF, and at 654 cm<sup>-1</sup>, on Zn-c-SBF, assigned for OH<sup>-</sup> bending vibration, were associated with others at 598 cm<sup>-1</sup>, on the former, and at 593 cm<sup>-1</sup>, on the latter, assigned for PO<sub>4</sub><sup>3-</sup> bending vibration  $\nu_4$ . This subsequently confirms the development of the apatite layer on the surface. Because the coating procedure was not vacuum sealed, peak appeared on both charts around 3108 cm<sup>-1</sup>, which is assigned for C-H bond. Here, it is clear how Sr incorporation accelerated the growth of the apatite in comparison to Zn.

### 10 Days Soaking

Stability, in the values of all peaks shown in these charts, is accompanied by a change in the carbonate to phosphate ratio with excess for the latter (Tables 3 and 4). The carbonate content here is ascribed to B-type which substitutes for phosphate groups rather than hydroxyl ones [34]. The sites assigned for strontianite or smithsonite continued their loss. This was accompanied by the decrement of carbonate content and increment in water and

**Table 3. Progress in the Optical Density Values of the Assignment Groups on Sr-c-SBF, Measured According to Kubelka-Munk Function**

Sr-c-SBF					
Group Assignment	Wavenumber $1/\lambda \text{ cm}^{-1}$	"Kubelka-Munk" Units			
		Sr-2p	Sr-3p	Sr-4p	Sr-5p
OH stretching vibration	3387	0.124	0.123	2.043	2.149
OH bending vibration	623 - 667	0.011	0.010	0.705	0.463
H-O-H scissors	1645	0.011	0.032	0.827	0.572
"C-O" stretch $\nu_3$	1394 - 1406	1.636	1.179	1.553	1.413
"out-of-plane" C-O bending vibration $\nu_2$	873	0.365	0.290	0.243	0.085
"in-plane" C-O bending vibration	710	0.023	0.018	0.051	0.057
$\text{PO}_4^{3-}$ stretching vibration $\nu_3$	1077	0.108	0.182	1.274	1.171
$\text{PO}_4^{3-}$ stretching vibration $\nu_1$	973	0.028	0.074	0.090	0.147
$\text{PO}_4^{3-}$ bending vibration $\nu_4$	562	0.008	0.014	0.038	0.088
$\text{PO}_4^{3-}$ bending vibration $\nu_2$	494	0.004	0.037	0.002	0.020
$\text{HPO}_4^{2-}$	767	0.010	0.004	0.007	0.021

hydroxyl content. This in turn claims that the grown phase is carbonated apatite [14,33,40]. Consequently, Sr and Zn could be responsible for inducing growth of this phase. The difference here lies in the mechanism and activity of incorporation. Sr induced faster growth by keeping the carbonate content and induced apatite formation by direct phosphate substitution. While Zn, just dropped down the carbonate content and then induced the mutual incorporation of both phosphate and carbonate groups. In comparison to our previous study concerning the conventional biomimetic coating [24], the incorporation of both Sr and Zn induced the growth of apatite with higher carbonate content. This is better from a biological point of view because the biological apatite is not highly crystalline hydroxyapatite. It is poorly

crystallized calcium-deficient as a result of various substitutions at regular HA lattice points. This is explained in details elsewhere [41].

### 3.2. SBF Solutions Analyses

#### $\text{Ca}^{+2}$ vs $iP$

The variation of both  $\text{Ca}^{+2}$  and  $iP$ , uptake onto the samples is given in Fig. (3). It is here assumed that any change by decrease/increase in calcium or phosphorus concentrations, with respect to mother solution, would represent a deposition/release on/from Sr-c-SBF or Zn-c-SBF surfaces respectively. In  $1.5 \times$  Sr-c-SBF solution, the alternative behavior of  $\text{Ca}^{+2}$  vs  $iP$  through successive soaking

**Table 4. The Progress in the Optical Density Values of the Assignment Groups on Zn-c-SBF, Measured According to Kubelka-Munk Function**

Zn-c-SBF					
Group Assignment	Wavenumber $1/\lambda \text{ cm}^{-1}$	"Kubelka-Munk" Units			
		Zn-2p	Zn-3p	Zn-4p	Zn-5p
OH stretching vibration	3387	0.031	0.053	0.766	2.049
OH bending vibration	626	0.019	0.010	0.345	0.458
H-O-H scissors	1635 - 1645	0.008	0.012	0.305	0.551
"C-O" stretch $\nu_3$	1400 - 1456	0.220	0.145	0.490	1.375
"out-of-plane" C-O bending vibration $\nu_2$	873	0.060	0.066	0.124	0.081
"in-plane" C-O bending vibration	710	0.017	0.011	0.060	0.045
$\text{PO}_4^{3-}$ stretching vibration $\nu_3$	1083	0.025	0.075	0.355	1.151
$\text{PO}_4^{3-}$ stretching vibration $\nu_1$	960	0.016	0.051	0.090	0.093
$\text{PO}_4^{3-}$ bending vibration $\nu_4$	562	0.015	0.014	0.069	0.090
$\text{PO}_4^{3-}$ bending vibration $\nu_2$	485	0.017	0.045	0.032	0.019
$\text{HPO}_4^{2-}$	767	0.011	0.005	0.066	0.019

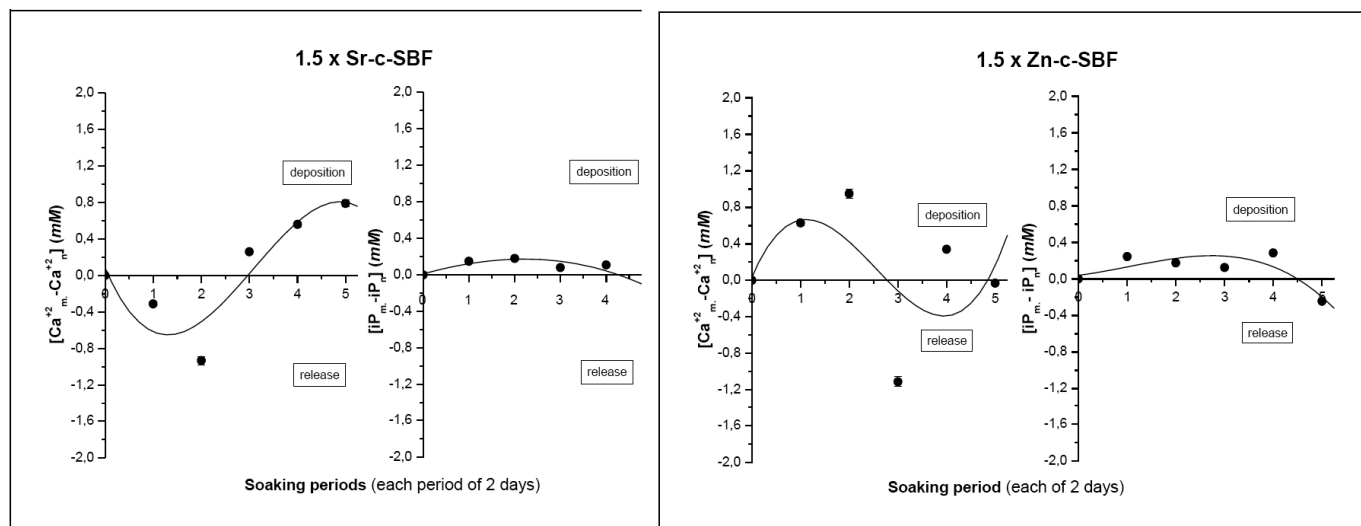


**Fig. (3).** Uptake of Ca<sup>+2</sup> & iP from 1.5×Sr-SBF and 1.5 × Zn-SBF post each soaking periods with respect to the mother solution. (Where, Ca<sup>+2</sup><sub>m</sub> & iP<sub>m</sub> are for mother solution, and, Ca<sup>+2</sup><sub>n</sub> & iP<sub>n</sub> are specific for each period). The drawn curves represent the polynomial fitting of the third order to the obtained results.

periods showed a deposition behavior. This agreed with the previously explained IR analyses, where, Sr-c-SBF kept the relatively high carbonate content in the initial periods and started earlier (than Zn-c-SBF) the phosphate deposition (Fig. 1). This explains why Ca<sup>+2</sup> showed in the soaking solutions higher values, indicating their release, followed by lower ones, indicating their deposition and contribution on the precalcified Sr-c-SBF surfaces [24]. On the other hand, an opposite trend was adopted in 1.5 × Zn-c-SBF. Ca<sup>+2</sup> started its deposition within the first soaking periods. This was synchronized by the release of the carbonate content as shown in IR analyses, (Fig. 2). When the carbonate content started to show some increment on Zn-c-SBF, starting from the third soaking period, a release behavior was recorded for Ca<sup>+2</sup>. The ideal alternative Ca<sup>+2</sup> - iP behavior is not shown in 1.5 × Zn-c-SBF [38].

**Ca<sup>+2</sup> vs Sr<sup>+2</sup>**

To visualize the exact influence of incorporation of Sr<sup>+2</sup> on the Ca<sup>+2</sup> behavior, a study of the variation of percentage fraction of Ca<sup>+2</sup> vs Sr<sup>+2</sup> through the successive soaking periods is shown (Fig. 4). The calculations were done with respect to the mother solution using atomic absorption spectroscopy. The diagram represents the values such that if they are lower than 100%, a decrement in ionic concentration is recorded, otherwise, there is an increment with respect to the mother solutions. As shown in the diagram, Ca<sup>+2</sup> and Sr<sup>+2</sup> behave oppositely. This accounts to the approximately similar ionic radii of Sr<sup>+2</sup> (1.13Å) and Ca<sup>+2</sup> (0.99 Å). This confirms our claim (explaining the IR charts) of the substitutional competition in the grown coating layer between both ions, consequently, giving an evidence of the contribution of Sr<sup>+2</sup> to the resultant biomimetic surface. Also, this shows quite “step-wise” agreement with IR data, (Fig. 1) in which it was apparent that the peaks that initially appeared on Sr-c-SBF, assigned for strontianite disappeared after the last soaking periods.

**Ca<sup>+2</sup> vs Zn<sup>+2</sup>**

The Ca/Sr competition is not really shown in case of Zn<sup>+2</sup> (Fig. 5). It started after about half the whole soaking

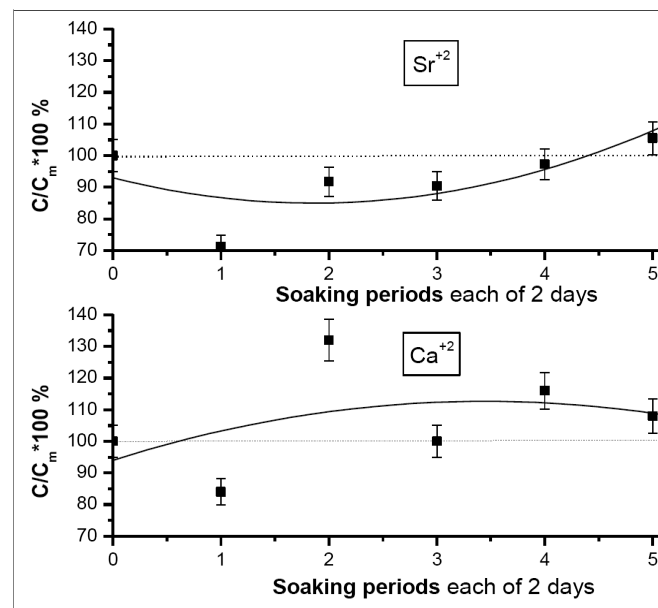


**Fig. (4).** Variation of the percentage fraction of Ca<sup>+2</sup> vs Sr<sup>+2</sup> post each soaking periods in 1.5 × Sr-c-SBF. The drawn curves represent the polynomial fitting of the second order to the obtained results.

procedure. From another point of view, this also indicates the interstitial incorporation of Zn<sup>+2</sup> into the grown apatite rather than the substitutional one. This is crystallographically true with respect to the ionic radius of Zn<sup>+2</sup> (0.83Å). Besides, this gives the other side of the story of the

disappearance of the peaks assigned for smithsonite during the progression of the soaking procedure, namely, in the second half of the process.

### Electrical conductivity

Conductivity measurement accounts to ionic concentrations of designed soaking solutions. In fact, the decrease in the ionic concentration, by their uptake from solution and

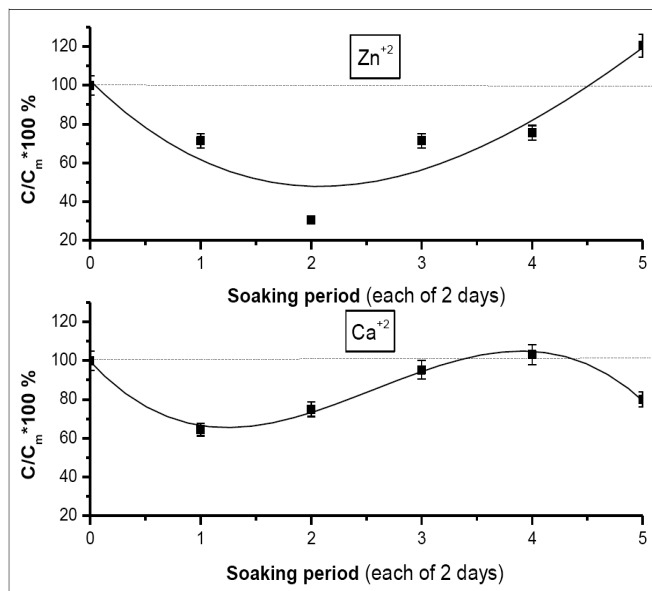


**Fig. (5).** Variation of percentage fraction of  $\text{Ca}^{+2}$  vs  $\text{Zn}^{+2}$  post each soaking periods in  $1.5 \times \text{Zn-SBF}$ . The drawn curve represents the polynomial fitting of the second order to the obtained results.

deposition onto the sample surface, would decrease the conductivity of the solution as a whole and vice versa. This would be represented as an “increased” decrement, in the following diagram (Fig. 6). For both solutions, the decrement slowed down gradually through the successive soaking periods. Although there was a starting resorption of the precalcified surface (shown earlier) which should have resulted in an overall increase in ionic concentration of the soaking solutions; this was compensated by the rapid uptake from SBFs. Besides, because we adopted a replenishment procedure of the soaking solutions, i.e., dynamic coating, this uptake decreased through the whole procedure with respect to the mother solution. The decrement of  $1.5 \times \text{Sr-c-SBF}$  was higher than that of  $1.5 \times \text{Zn-c-SBF}$ . This consequently shows the superiority of  $\text{Sr}^{+2}$  over  $\text{Zn}^{+2}$ . After six days soaking, which corresponded to carbonate/phosphate substitution on Sr-c-SBF (Fig. 1), the conductivity started its increase, indicating dissolution. But, this was slightly changed after the fifth soaking period, which corresponded to more progression and differentiation of the phosphate bands on Sr-c-SBF. The conductivity trend showed a start of a new cycle of deposition (after 10 days soaking) and therefore, assures the continuity of the apatite growth. Therefore, Sr-c-SBF showed a desiring attitude for more depositions confirming, its bone seeking behavior [44]. In contrast,  $1.5 \times \text{Zn-c-SBF}$  continued overall increase in the

ionic concentration in the last soaking periods, indicating an overall dissolution mechanism.

### Ionic product $Q_{sp}$ Studies

$\text{Ca}^{+2}$  and iP ionic concentrations (Table 5) of soaking solutions interpret the real situation of apatite deposition. The surface was initially calcium rich due to pre-calcification [24]. The positively charged surface started to attract the negative phosphate ions. This was followed by the formation of a calcium poor, negatively charged surface that once again attracted the positive divalent calcium ions from the SBF. Consequently, an amorphous calcium phosphate phase was formed on the alloy surface. This in turn had undergone more deposition accompanied by selective dissolutions to reach the real poorly crystallized apatite that mimics the biological apatite. An important measurement would be the ionic product,  $Q_{sp}$ . (Fig. 7) illustrates the decrement of  $[\text{Ca}^{+2} + \text{Sr}^{+2}][\text{iP}]$  and  $[\text{Ca}^{+2} + \text{Zn}^{+2}][\text{iP}]$  through the successive soaking periods with respect to their mother solutions. The higher the values’ positivity, the higher the decrement in the ionic product.  $1.5 \times \text{Sr-c-SBF}$  showed lower decrement than that of  $1.5 \times \text{Zn-c-SBF}$  (Fig. 7). Therefore, the supersaturation level was kept at higher values for the former than the latter. According to the non classical theory of homogenous nucleation, indirect rapid and higher crystallization of amorphous calcium phosphates would be expected on Sr-c-SBF compared to Zn-c-SBF. In great resemblance, these results are in a general consistent with those of electrical conductivity (Fig. 6).

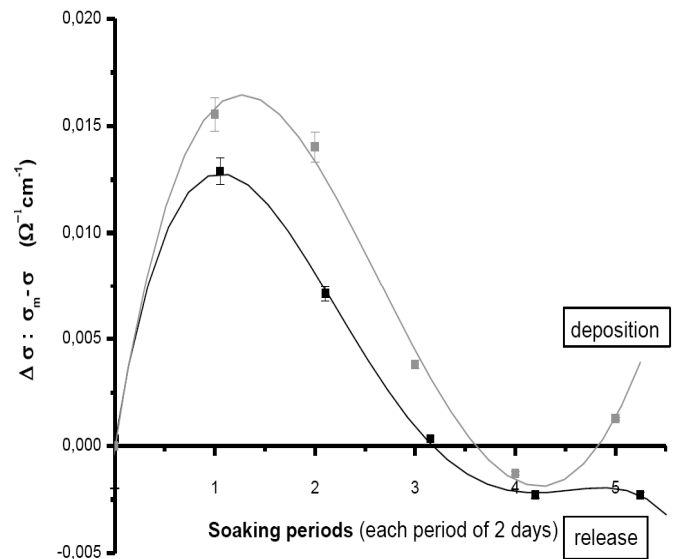


**Fig. (6).** Decrement in electrical conductivity of  $1.5 \times \text{Sr-SBF}$  (grey) and  $1.5 \times \text{Zn-SBF}$  (black) through various soaking periods with respect to the mother solution. (Where  $\sigma_m$  is the conductivity of the mother solution and  $\sigma_n$  is the conductivity of respective time interval). The drawn curve represents the polynomial fitting of fourth order to the obtained results.

Compared to control treatment [24],  $\text{Sr}^{+2}$  and  $\text{Zn}^{+2}$  retarded the growth of highly dense apatite phase on Ti-6Al-4V, especially for the former. They also increased the calcium deficiency in the resultant phase. This can be easily explained through the assessment of the values of  $\text{Ca}^{+2} + \text{Sr}^{+2}/\text{iP}$  and  $\text{Ca}^{+2} + \text{Zn}^{+2}/\text{iP}$  (Table 5). Chou *et al.* [42] indicated that amorphous calcium phosphate, ACP, (25%

**Table 5.** Measured Values of Ca<sup>+2</sup>, Sr<sup>+2</sup>, Zn<sup>+2</sup>, iP and their Total Ratio in Modified Sr and Zn Containing SBF

Solution	1.5 x Sr-c-SBF				1.5 x Zn-c-SBF			
	Ca <sup>+2</sup> (mM)	Sr <sup>+2</sup> (mM)	iP (mM)	[Ca <sup>+2</sup> + Sr <sup>+2</sup> ]/iP	Ca <sup>+2</sup> (mM)	Zn <sup>+2</sup> (mM)	iP (mM)	[Ca <sup>+2</sup> + Zn <sup>+2</sup> ]/iP
Zero	3.10	0.50	1.23	2.93	3.10	0.49	1.06	3.42
1 <sup>st</sup>	2.57	0.36	1.08	2.71	2.00	0.35	0.81	2.91
2 <sup>nd</sup>	4.05	0.46	1.05	4.29	2.32	0.15	0.88	2.81
3 <sup>rd</sup>	3.13	0.45	1.15	3.11	2.95	0.35	0.93	3.56
4 <sup>th</sup>	3.63	0.49	1.12	3.68	3.20	0.37	0.77	4.64
5 <sup>th</sup>	3.33	0.53	1.40	2.76	2.48	0.59	1.30	2.37

crystallinity) showed a higher biosolubility than standard HA (63% crystallinity) and the lower crystallinity might be favorable to cell attachment. However, high biosolubility of ACP resulted in an increased pH of culture medium up to 8.2, which inhibited the proliferation of attached cells. Therefore, a balance between the phase structure (crystallinity) and its biosolubility should be considered.

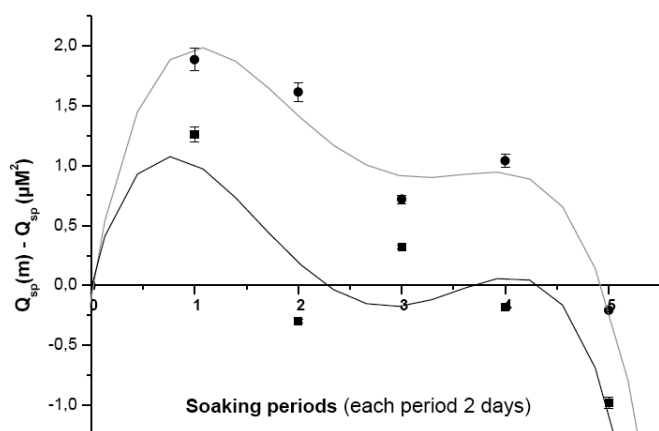


**Fig. (7).** The decrement of [Ca<sup>+2</sup>+Sr<sup>+2</sup>]/iP, black, and [Ca<sup>+2</sup>+Zn<sup>+2</sup>]/iP, red, post each soaking period with respect to their mother solutions. The polynomial fitting here is of the fourth order.

### 3.3. Morphology Assessment

The surface morphologies of Sr-c-SBF and Zn-c-SBF post the whole coating periods are shown in (Fig. 8). The coatings appeared to completely cover the sample surface. The surfaces show irregularities, multilayered structures and multiple phase growth which is attributed to the successive dynamic coating.

Sr-c-SBF showed irregular deposits grown on their surfaces. At low magnification (x800), plate-like and rod-like structures are stabilized on the surface (Fig. 8a, b). At higher magnification (x1500), (Fig. 8c, d), few tiny spheroid structures of diameter ranges from 2μm to 3.5μm are randomly distributed throughout the surface. Such tiny rounded structures account for the growth of nanoapatitic phases. It was reported previously that strontium incorporation inhibited the growth of the apatite crystals leading to the formation of carbonated nano-apatitic crystals [35]. The apparent irregular structures could be attributed to the growth of brushite [43]. Nucleation of strontium-substituted apatite might be easier than standard biological apatite. It

could act as a template for the formation of new bone, even with its metastable nature. Thus, new bone growth might be promoted when strontium is released from the implant surface.

On Zn-c-SBF, uniform coating is observed. It exhibits characteristic interlocking, microrod-like structures (Fig. 8e, f). The surface also showed tiny spherical morphology randomly grown on the surface (Fig. 8f). At higher magnification (x3500), some semispherical calcium phosphate globules (or spherulites) appear to be attached on these neat micro-rods (Fig. 8g). They vary in diameter from 1.72 μm to 6.90 μm (Fig. 6h). Such micro rods went through a process of low level surface dissolution - reprecipitation during the successive soaking periods. This may account for their maintenance of their rod-like nature [44]. The relatively large surface area of these microrods is expected to enhance more deposition onto the sample surface. This would recommend future studies concerning antibacterial and antimicrobial effects. An atomic-level incorporation mechanism of Zn<sup>+2</sup> in HA can take place through occupying the Ca<sup>+2</sup> vacancy of the defect complex. Not only is Ca<sup>+2</sup> vacancy complex an origin of calcium deficiency of HA, but also plays a key role in the uptake of trace elements during mineralization. Normally biological apatite is described as a carbonate apatite and is liable to contain many “foreign” species. Here, DRIFTS showed an obvious adsorption peak for carbonate, arising from the 4.2 mM HCO<sub>3</sub><sup>-1</sup> in the SBF solution. This presence is due to substitution for phosphate, as indicated by the increased (Ca + Sr)/P ratio (>2.0) (Table 5) and this is what we expect to occur in a physiological environment.

### 4. CONCLUSIONS

In the present study, we propose a novel method for incorporating trace element, like Sr and Zn, into the apatite grown on Ti-6Al-4V. Instead of using “two-step” route; preparing Sr or Zn substituted hydroxyapatite powder followed by using relatively complicated methods, like plasma spraying or pulsed laser deposition, to deposit the resultant phase on the alloy surface; we here adopt a very simple “one-step” route, by allowing the simultaneous incorporation of Ca<sup>+2</sup> and Sr<sup>+2</sup> or Zn<sup>+2</sup> onto the grown layer in a modified SBF. Sr<sup>+2</sup> and Zn<sup>+2</sup> showed their trend to retard the growth of highly mature crystalline apatite. Both, Sr and Zn modified SBF induced the growth of carbonate rich apatite, being of higher HCO<sub>3</sub><sup>-</sup> content in the former than the latter. Sr increased the deposition activity, when compared to

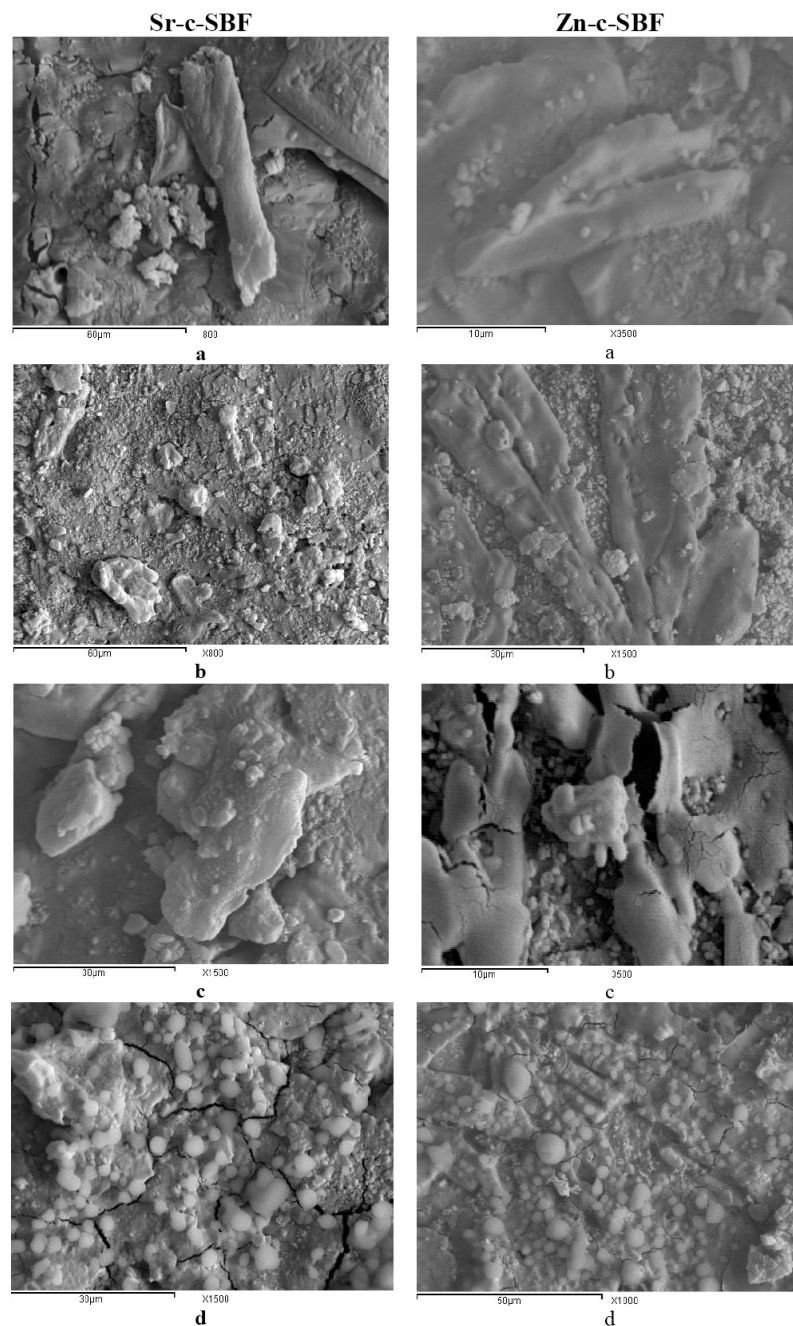


**Fig. (8).** SEM micrographs of Sr-c-SBF and Zn-c-SBF at several degrees of magnification. On Sr-c-SBF, agglomerations of semi plate structures dominate, (a, b, c) together with very tiny spherical structures, (d), confirm the proceeding of the coating procedure. On Zn-c-SBF, micro rods, (e, f, g), and tiny spherical structures, (h), are shown to cover the surface.

Zn, which may regard to its bone seeking attitude. While Zn modified SBF adopted the conventional mechanism of biomimetic coating on the precalcified alloy, being dissolution-precipitation, Sr modified SBF choose another mechanism, being substitution. The results derived from DRIFTS and SEM, confirm that the higher the carbonate content, the lower the uniformity of the resultant apatite layer. Besides, the solution analysis was very useful in order to get the complementary information of the coating procedure. Further *in vitro* studies are required to assess the precise effects due to the individual presence of these trace elements or their combined effects on the improvement of implants “bio” functionality.

#### ACKNOWLEDGEMENT

The work is part of the research presented by Alaa Adawy in her defense for the master degree. The authors would like to thank the cooperation of the central laboratories at Faculty of science, Ain Shams University and NRC, Cairo, Egypt, for enabling their instrumental support.

#### REFERENCES

- [1] Lee H-R. Comparative study of bond characteristics between Titanium/Titanium alloy and ceramic, Ph.D Thesis. Yeosu, Korea 2004; p. 14.
- [2] José W, Guilherme G, Henriques PE, Junior T M, Mesquita FM, Dezan CC. Evaluation of low-fusing ceramic systems combined

- with titanium grades II and V by bending test and scanning electron microscopy. *J Appl Oral Sci* 2003;11 (4): 354-60.
- [3] Lin J-H, Chang C-H, Chen Y-S, Lin G-T. Formation of bone-like apatite on titanium filaments incubated in a simulated body fluid by using an electrochemical method. *Compos A* 2007; 38 (2): 535-9.
- [4] Ban S, Maruno S. Morphology and microstructure of electrochemically deposited calcium phosphates in a modified simulated body fluid. *Biomaterials* 1998; 19: 1245-53.
- [5] Dong ZL, Khor A, Quek CH, White TJ, Cheang P. TEM and STEM analysis on heat treated and *in vitro* plasma sprayed hydroxyapatite/Ti-6Al-4V composite coatings. *Biomaterials* 2003; 24: 97-105.
- [6] Hench L L. Bioceramics. *J Am Ceram Soc* 1998; 81(7): 1705-28.
- [7] Wang S-H, Shih W-J, Li W-L, Hon M-H, Wang M-C. Morphology of calcium phosphate coatings deposited on a Ti-6Al-4V substrate by an electrolytic method under 80 Torr. *J Eu Ceram Soc* 2005; 25: 3287- 3292.
- [8] Leventouri T. Synthetic and biological hydroxyapatites: Crystal structure questions. *Biomaterials* 2006; 27: 3339-42.
- [9] Kokubo T, Kim H, Kawashita M. Novel bioactive materials with different mechanical properties. *Biomaterials* 2003; 24(13): 2161-7.
- [10] Rigo CS, Boschi AO, Yoshimoto M, Allegrini Jr S, Konig Jr B, Carbonari M J. Evaluation *in vitro* and *in vivo* of biomimetic hydroxyapatite coated on titanium dental implants. *Mater Sci Eng C* 2004; 24: 647-651.
- [11] Lu X, Leng Y. Theoretical analysis of calcium phosphate precipitation in simulated body fluid. *Biomaterials* 2005; 26:1097.
- [12] Barrere F, Snel MME, van Blitterswijk CA, de Groot K, Layrolle P. Nano-scale study of the nucleation and growth of calcium phosphate coating on titanium implants. *Biomaterials J* 2004; 25: 2901-2910.
- [13] Bharati S, Sinha MK, Basub D. Hydroxyapatite coating by biomimetic method on titanium alloy using concentrated SBF. *Bull Mater Sci* 2005; 28(6): 617-21.
- [14] Hu K, Yang X-J, Cai Y-L, Cui Z-D, Wei Q. Preparation of bone-like composite coating using a modified simulated body fluid with high Ca and P concentration. *Surf Coat Technol* 2006; 201:1902-6.
- [15] Bertoni E, Bigi A, Cojazzi G, Gandolfi M, Panzavolta S, Rover N. Nanocrystals of magnesium and fluoride substituted hydroxyapatite. *J Inorg Biochem* 1998; 72: 29-35.
- [16] Compston J. Guidelines for the management of osteoporosis: the present and the future. *Osteoporos Int* 2005; 16(10): 1173-6.
- [17] Marie PJ. Strontium ranelate: A physiological approach for optimizing bone formation and resorption. *Bone* 2006; 38(2): 10-14.
- [18] Kendler DL. Strontium ranelate—data on vertebral and non vertebral fracture efficacy and safety: mechanism of action. *Curr Osteoporos Rep* 2006; 4: 34-9.
- [19] Boivin G, Deloffre P, Perrat B, *et al.* Strontium distribution and interactions with bone mineral in monkey iliac bone after strontium salt (S 12911) administration. *J Bone Miner Res* 1996; 11: 1302-11.
- [20] Li Z Y, Lam W M, Yang C, *et al.* Chemical composition, crystal size and lattice structural changes after incorporation of strontium into biomimetic apatite. *Biomaterials* 2007; 28: 1452-1460.
- [21] Hashizume M, Yamaguchi M. Stimulatory effect of beta-alanyl-L-histidinato zinc on cell proliferation is dependent on protein synthesis in osteoblastic MC3T3-E1 cells. *Mol Cell Biochem* 1993; 12: 122-59.
- [22] Miao S, Weng W, Cheng K, Du P, Shen G, Han G, Zhang S. Sol-gel preparation of Zn-doped fluoridated hydroxyapatite films. *Surf Coat Technol* 2005; 198: 223-6.
- [23] Grandjean-Laquerriere A, Laquerriere P, Jallot E, *et al.* Influence of the zinc concentration of sol-gel derived zinc substituted hydroxyapatite on cytokine production by human monocytes *in vitro*. *Biomaterials* 2006; 27: 3195-200.
- [24] Adawy A, Abd El-Fattah WI, El-Sayed E-SM, Talaat MS. Biomimetic coating of precalcified Ti-6Al-4V alloy. *J Open Med Devices* 2009; 1:19-28.
- [25] Kokubo T, Takadama H. How useful is SBF in predicting *in vivo* bone bioactivity? *Biomaterials* 2006; 27: 2907-15.
- [26] Kortum G. Reflectance spectroscopy. Springer-Verlag: New York. 1969.
- [27] Ghauch A, Rima J, Charef A, Suptil J, Fachinger C, Martin-Bouyer M. Quantitative measurements of ammonium, hydrogenophosphate and Cu(II) by diffuse reflectance spectrometry. *Talanta* 1999; 48: 385-92.
- [28] Bayraktar D, Tas AC. Chemical preparation of carbonated calcium hydroxyapatite powders at 37°C in urea-containing synthetic body fluids. *J Eur Ceram Soc* 1999; 19: 2573-1979.
- [29] Barrere F, van Blitterswijk C A, de Groot K, Layrolle P. Nucleation of biomimetic Ca-P coatings on Ti6Al4V from a SBF×5 solution: influence of magnesium. *Biomaterials* 2002; 23: 2211-20.
- [30] Habibovic P, Barrere F, van Blitterswijk CA, de Groot K, Layrolle P. Biomimetic hydroxyapatite coating on Metal implants. *J Am Ceram Soc* 2002; 85: 517-22.
- [31] Ng BS, Annergren I, Soutar AM, Khor KA, Jarfors AEW. Characterization of a duplex TiO<sub>2</sub>/CaP coating on Ti6Al4V for hard tissue replacement. *Biomaterials* 2005; 26: 1087-1095.
- [32] Habibovic P, Li J, van der Valk M C, Meijer G, Layrolle P, van Blitterswijk CA, de Groot K. Biological performance of uncoated and octacalcium phosphate-coated Ti6Al4V. *Biomaterials* 2005; 26: 23-36.
- [33] Müller L, Müller FA. Preparation of SBF with different HCO<sub>3</sub><sup>-</sup> content and its influence on the composition of biomimetic apatites. *Acta Biomater* 2006; 2: 181-9.
- [34] Murugan R, Ramakrishna S. Production of ultra-fine bioresorbable carbonated hydroxyapatite. *Acta Biomater* 2006; 2: 201-6.
- [35] Oliveira AL, Reis RL, Li P. Strontium-substituted apatite coating grown on Ti6Al4V substrate through biomimetic synthesis. *J Biomed Mater Res Part B: Appl Biomaterials* 2007; 83B: 258-65.
- [36] Smith B. Infrared spectral interpretation: A systematic approach. USA: CRC Press 1998.
- [37] Chou Y-F, Chiou W-A, Xu Y, Dunn J CY, Wu B M. The effect of pH on the structural evolution of accelerated biomimetic apatite. *Biomaterials* 2004; 25: 5323-31.
- [38] Greigor RB, Jr N E P, Lytle F I W. Strontianite in coral skeletal aragonite. *Science* 1997; 275: 1452-4.
- [39] Kitano Y, Kanamori N, Yoshioka S. Adsorption of zinc and copper ions on calcite and aragonite and its influence on the transformation of aragonite to calcite. *Geochem J* 1976; 10: 175-9.
- [40] Wang J, Layrolle P, Stigter M, de Groot K. Biomimetic and electrolytic calcium phosphate coatings on titanium alloy: physicochemical characteristics and cell attachment. *Biomaterials* 2004; 25: 583-92.
- [41] Shi D. Biomaterials tissue and engineering. Springer-Verlag: Berlin Heidelberg 2004.
- [42] Chou L, Marek B, Wagner W R. Effects of hydroxylapatite coating crystallinity on biosolubility, cell attachment efficiency and proliferation *in vitro*. *Biomaterials* 1999; 20(10): 977-85.
- [43] Tas AC. Electroless deposition of brushite (CaHPO<sub>4</sub>·2H<sub>2</sub>O) crystals on Ti-6Al-4V at room temperature. *J Mater Res* 2006; 97(5): 639-44.
- [44] Jalota S, Bhaduri S B, Tas A C. Using a synthetic body fluid (SBF) solution of 27 mM HCO<sub>3</sub><sup>-</sup> to make bone substitutes more osteointegrative. *Mater Sci Eng C* 2008; 28: 129-140

Received: May 25, 2009

Revised: November 24, 2010

Accepted: December 3, 2010

© Abdel-Fattah *et al.*; Licensee Bentham Open.This is an open access article licensed under the terms of the Creative Commons Attribution Non-Commercial License (<http://creativecommons.org/licenses/by-nc/3.0/>) which permits unrestricted, non-commercial use, distribution and reproduction in any medium, provided the work is properly cited.